Anomalous thermal Hall conductivity of ferromagnetic transition metals

Insu Baek,[1] Kyoung-Whan Kim,[2,3] Jung Hoon Han,[4] and Hyun-Woo Lee[1,*]
[1]*Department of Physics, Pohang University of Science and Technology, Pohang 37673, Korea*
[2]*Center of Spintronics, Korea Institute of Science and Technology, Seoul 02792, Korea*
[3]*Department of Physics, Yonsei University, Seoul 03722, Korea*
[4]*Department of Physics, Sungkyunkwan University, Suwon 16419, Korea*

(Received 18 November 2023; revised 31 January 2024; accepted 21 February 2024; published 11 March 2024)

In ferromagnetic metals where the anomalous Hall effect (AHE) occurs, one expects a corresponding thermal Hall transport due to electrons that may be dubbed the anomalous thermal Hall effect (ATHE). The same mechanisms that are responsible for AHE, such as the intrinsic Berry curvature effect (usually the most important) or the side-jump mechanism, should play significant roles in ATHE as well. Despite the obvious correlations between AHE and ATHE expected on generalized Wiedemann-Franz law, however, the actual thermal Hall conductivities from each of these contributions have not been evaluated quantitatively. Here, we investigate the intrinsic and the impurity-scattering-induced side-jump contributions to the AHE and the ATHE in 3*d* ferromagnetic metals, bcc Fe, hcp Co, and fcc Ni. We find that the sum of the intrinsic and the side-jump contributions to anomalous thermal Hall conductivity (ATHC) agrees with the experimental values in Fe and Co rather well. In Ni, the calculated ATHC is much larger than the experimental value. We attribute this difference to the importance of electron-phonon scattering in Ni.

DOI: 10.1103/PhysRevB.109.115113

I. INTRODUCTION

The thermal Hall effect (THE), the emergence of transverse heat current when a longitudinal temperature gradient is applied, has attracted a lot of recent attention. THE is generally reported in insulators [1–5], where only the charge-neutral quasiparticles can transport heat. The carriers are believed to be magnons [6,7], phonons [4,5,8–10], or some exotic fractionalized particles [3,11] depending on the material in question.

In stark contrast to observation and theory of THE in insulators, analogous discussion for metals has rarely taken place. This is understandable, given that the carriers are predominantly electrons, and both electricity and heat are carried by the same electrons according to the Wiedemann-Franz law [12]. Indeed, the early measurements on the anomalous Hall conductivity and the thermal Hall conductivity in magnetic metals have been interpreted in this way [13,14]. It does not imply, however, that the naive application of the Wiedemann-Franz law is justified in the case of anomalous Hall electric and thermal transports. The purpose of this paper is to theoretically investigate this question.

As is well known, electric Hall transport in magnetic metals has two parts, one arising from the normal Hall effect under the magnetic field and the other anomalous part due to the magnetization [15]. The latter phenomenon is known as the anomalous Hall effect (AHE) [Fig. 1(a)]. Accordingly, the thermal Hall conduction must also consist of the normal and the anomalous parts, with the latter appropriately dubbed the anomalous thermal Hall effect of ATHE [Fig. 1(b)]. It is also natural to infer that various mechanisms responsible for AHE, such as the Berry curvature effect, skew scattering, and side jump, will have corresponding contributions to the thermal Hall conduction as well. Although it has been common to believe that ATHE and AHE together obey the Wiedemann-Franz law [12], called the anomalous transverse Wiedemann-Franz law, it was recently reported that the anomalous transverse Wiedemann-Franz law could be violated at room temperature [16] due to the effects of the intricate electronic band structure. Thus, it is of both fundamental and practical importance to quantitatively check whether the anomalous transverse Wiedemann-Franz law holds over various temperatures. The previously calculated anomalous Hall conductivity (AHC) of 3*d* ferromagnetic transition metals such as Fe, Co, and Ni shows a quantitative fit to the experimental results [17–19]. Here, we ask if a similar quantitative understanding of the ATHE is also possible.

With this motivation, we calculate the intrinsic and side-jump contributions to the ATHE for 3*d* ferromagnetic metals, bcc Fe, hcp Co, and fcc Ni using the first-principle calculations through the density functional theory with the on-site Hubbard U correction (DFT+U) [20–22]. In ferromagnetic metals with longitudinal electrical conductivity in the range 10^3–10^6 $(\Omega\,\mathrm{cm})^{-1}$, which include most moderately dirty metals, the AHE is dominated by the Berry-curvature-induced intrinsic mechanism, followed by the contribution from the side-jump mechanism [15]. Both contributions are independent of the disorder potential strength. It was both theoretically predicted and experimentally measured that the skew scattering mechanism negligibly contributes to the AHE in $T > 100$ K [12–14]. The electron self-energy, including

*hwl@postech.ac.kr

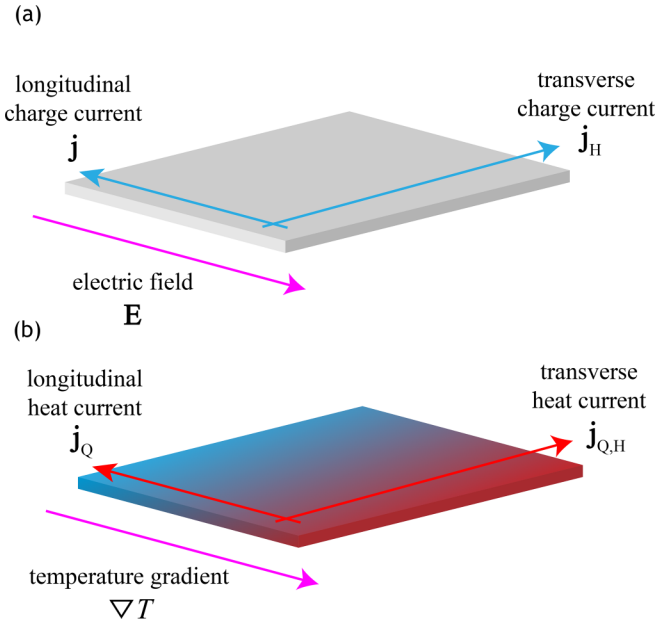

FIG. 1. Schematic representation of the AHE (a) and the ATHE (b).

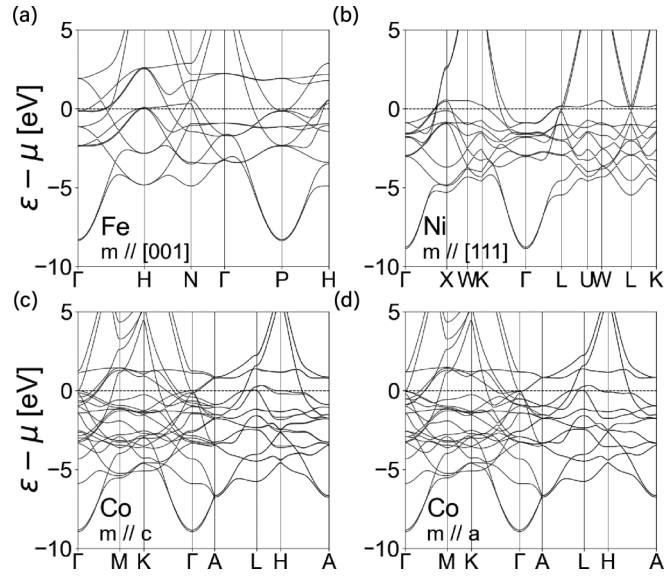

FIG. 2. Band structures of bcc Fe (a), fcc Ni (b), and hcp Co (c) (d). Each element is magnetized along [001] (a), [111] (b), *c* axis (c), and *a* axis (d). The true Fermi energy is $\varepsilon = \mu$.

the electron-phonon interaction, can enhance the accuracy of the AHC calculation. Still, the cost of its application to the first-principle calculation is expensive [23]. In 3*d* ferromagnetic metals, the electron-phonon scattering barely contributes to the AHC except for fcc Ni, so the DFT+U calculation is enough to obtain the AHC in accuracy [24]. Thus, the AHC calculation without considering the skew scattering or the electron-phonon scattering would be quite accurate for the experiment, and this would be held in the ATHC since the ATHC follows the AHC. Here, we simply assume that the former two mechanisms are the two leading contributions for the anomalous thermal Hall conductivity (ATHC) κ_H. Our findings reveal that when considering both the intrinsic and impurity-scattering-induced side-jump contributions, the calculated ATHC agrees well with experimentally measured values for Fe and Co. With Ni, on the other hand, the collective effect of intrinsic and impurity-related side-jump factors leads to a notable deviation from the experimental value. This discrepancy is attributed to the substantial impact of electron-phonon scattering on the ATHC in Ni.

Some caveats of our calculations are the following. For the side-jump contribution, we take into account the electron side jump caused by impurity scattering but not by electron-phonon interaction [25]. This restriction to the impurity scattering effects is justified at low temperatures where the phonon population is small or in materials with weak electron-phonon coupling. Indeed, in Ni, where the electron-phonon coupling is strong, the calculated AHE deviates from the experimental value. In contrast, in the materials where electron-phonon scattering is weak, like Fe and Co, the calculated AHE quantitatively matches the experimental results. The ATHE calculation we present follows similar trends.

This paper is organized as follows. In Sec. II, the calculation methods used in this paper are introduced. In Sec. III, we compare our calculation results for anomalous Hall conductivity (AHC) to the previous calculation results and experimental results to check the validity of our calculation scheme. In Sec. IV, we present our calculation results for the ATHC and argue that our studies for ATHC agree with the previous experiments. In Sec. V, we quantitatively examine the validity of the Wiedemann-Franz law for AHC and ATHC. Section VI summarizes this paper.

II. FORMULATION

We proceed with the DFT+U calculation for bcc Fe, hcp Co, and fcc Ni in the following manner. Initially, we obtain the self-consistent electronic structures using QUANTUM ESPRESSO 6.6 [26]. We use Perdew-Burke-Ernzerhof exchange-correlation functional based on the generalized gradient approximation (GGA) with norm-conserving pseudopotentials [27,28]. The Brillouin zone is sampled using the $12 \times 12 \times 12$ Monkhorst-Pack **k**-point mesh [29]. We adopt Dudarev's scheme [22] to include the Hubbard term U and the Hund exchange term J. Specifically, we select the values for U and J as follows: $U = J = 0$ for Fe [30], $U = 1.6$, $J = 0.9$ for Co [18], $U = 1.9$, $J = 1.2$ for Ni [31] in electron volts (eV), primarily because using these values reproduce the measured AHC very well. The lattice constants are $a = 2.83$ for bcc Fe [32], $a = 2.50$, $c = 4.03$ [33] for hcp Co, and $a = 3.52$ [34] for fcc Ni in angstrom (Å), respectively. The resulting bcc Fe, fcc Ni, and hcp Co band structures are presented in Fig. 2. Co has a large anisotropy between the two magnetization directions: *c* axis and *a* axis. The anisotropy between *a* axis and *b* axis is expected to be much smaller by comparison, and we calculate the band structures only for *c*- and *a*-axis magnetization.

Next, we obtain the maximally localized Wannier functions (MLWFs) from the Bloch states with WANNIER90 code [35]. The Brillouin zone is sampled with the equidistant $12 \times 12 \times 12$ **k** mesh, including the Γ point. The Bloch states are initially

projected into s, p_x, p_y, p_z, d_{xy}, d_{yz}, d_{xz}, $d_{x^2-y^2}$, and d_{z^2} states. We obtained 18 MLWFs (bcc Fe, fcc Ni) out of 54 bands and 36 MLWFs (hcp Co) out of 108 bands. The frozen windows for the MLWF determination are set to include a region 4 eV higher than the true Fermi energy.

We employ the Kubo formula to evaluate the intrinsic portions of AHC ($\sigma_{\mathrm{H}}^{\mathrm{int}}$) and ATHC ($\kappa_{\mathrm{H}}^{\mathrm{int}}$) given by [36]

$$\sigma_{\mathrm{H},\alpha\beta}^{\mathrm{int}} = \frac{e^2}{\hbar}\sum_{n\neq m}\int \frac{d^3\mathbf{k}}{(2\pi)^3}(f_{m\mathbf{k}} - f_{n\mathbf{k}})\Omega_{nm\mathbf{k}}^{\alpha\beta}, \tag{1a}$$

$$\frac{\kappa_{\mathrm{H},\alpha\beta}^{\mathrm{int}}}{T} = \frac{k_{\mathrm{B}}^2}{\hbar}\sum_{n\neq m}\int \frac{d^3\mathbf{k}}{(2\pi)^3}[c_2(f_{m\mathbf{k}}) - c_2(f_{n\mathbf{k}})]\Omega_{nm\mathbf{k}}^{\alpha\beta}, \tag{1b}$$

$$\Omega_{nm\mathbf{k}}^{\alpha\beta} = \hbar^2\,\mathrm{Im}\left[\frac{\langle u_{n\mathbf{k}}|\, v_\beta\, |u_{m\mathbf{k}}\rangle\,\langle u_{m\mathbf{k}}|\, v_\alpha\, |u_{n\mathbf{k}}\rangle}{(\varepsilon_{n\mathbf{k}} - \varepsilon_{m\mathbf{k}})^2}\right], \tag{1c}$$

where n and m are band indices, k_{B} is the Boltzmann constant, v_α is α component of the velocity operator, $f_{n\mathbf{k}}$ is the Fermi-Dirac distribution function, $|u_{n\mathbf{k}}\rangle$ is the periodic part of the Bloch state with the energy eigenvalue $\varepsilon_{n\mathbf{k}}$, and $c_2(f_{n\mathbf{k}}) = \int_0^{f_{n\mathbf{k}}} (\log(t^{-1}-1))^2\, dt$.

We also evaluate the impurity-scattering-induced side-jump contributions to AHC [37] ($\sigma_{\mathrm{H}}^{\mathrm{sj}}$) and ATHC ($\kappa_{\mathrm{H}}^{\mathrm{sj}}$). In the weak disorder limit, this contribution can be evaluated by the formulas given by

$$\sigma_{\mathrm{H},\alpha\beta}^{\mathrm{sj}} = \frac{e^2}{\hbar}\sum_n \int \frac{d^3\mathbf{k}}{(2\pi)^3}\partial_\varepsilon f_{n\mathbf{k}}\,\mathrm{ReTr}\times\left\{\frac{\gamma_c}{[\gamma_c]_{nn}}\left[S_n A_{k_\alpha}(1-S_n)\frac{\partial\varepsilon_n}{\partial\varepsilon_\beta} - (\alpha\leftrightarrow\beta)\right]\right\}, \tag{2a}$$

$$\frac{\kappa_{\mathrm{H},\alpha\beta}^{\mathrm{sj}}}{T} = \frac{k_B^2}{\hbar}\sum_n \int \frac{d^3\mathbf{k}}{(2\pi)^3}\partial_\varepsilon c_2(f_{n\mathbf{k}})\,\mathrm{ReTr}\times\left\{\frac{\gamma_c}{[\gamma_c]_{nn}}\left[S_n A_{k_\alpha}(1-S_n)\frac{\partial\varepsilon_n}{\partial\varepsilon_\beta} - (\alpha\leftrightarrow\beta)\right]\right\}, \tag{2b}$$

Here, γ_c is a $\mathbf{k}$-dependent matrix defined as $\gamma_c(\mathbf{k}) = U^\dagger(\mathbf{k})\gamma U(\mathbf{k})$ where $\gamma = \pi\sum_n \int \frac{d^3\mathbf{k}'}{(2\pi)^3}U(\mathbf{k}')S_n U^\dagger(\mathbf{k}')\delta(\varepsilon - \varepsilon_{n\mathbf{k}'})$. The scattering strength does not appear explicitly in the side-jump formula [38]. The side-jump contribution $\kappa_{\mathrm{H},\alpha\beta}^{\mathrm{sj}}$ to the ATHC in Eq. (2b) is evaluated from the generalized Wiedemann-Franz law [39–41],

$$\kappa = \frac{1}{e^2 T}\int (\varepsilon-\mu)^2\frac{df(\varepsilon-\mu)}{d\varepsilon}\sigma_{T=0}(\varepsilon). \tag{3}$$

The impurity-scattering-dependent side-jump anomalous Nernst conductivity was calculated [31] using the same Mott formula. In the above formulas, $[S_n]_{ij} = \delta_{ij}\delta_{in}$, ε is the Fermi energy, $U(\mathbf{k})$ is a unitary matrix at point $\mathbf{k}$ that diagonalizes the Hamiltonian $H(\mathbf{k})$, $[U^\dagger H(\mathbf{k})U]_{nm} = \varepsilon_{n\mathbf{k}}\delta_{nm}$, and $A_{k_\alpha} = iU^\dagger\partial_{k_\alpha}U$ is the interband Berry connection matrix. The $\mathbf{k}$ integration in Eqs. (1) and (2) is calculated using uniformly distributed $240\times240\times240$ $\mathbf{k}$-mesh grid. The AHC and ATHC are calculated by increasing ε from $\mu - 0.5$ eV to $\mu + 0.5$ eV with 0.01 eV step, where the true Fermi energy is set to $\varepsilon = \mu$. The temperature dependence is included only in $f_{n\mathbf{k}}$. The electron-phonon interaction is ignored in these equations.

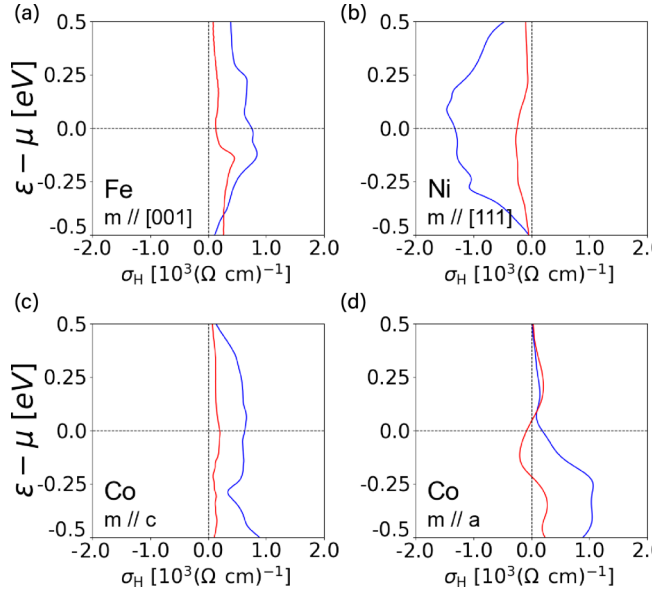

FIG. 3. The AHC from the intrinsic mechanism (blue line) and the impurity-scattering-induced side-jump mechanism (red line) of bcc Fe [001] (a), fcc Ni [111] (b), and hcp Co magnetized along c axis (c) and a axis (d) at $T = 150$ K.

III. ANOMALOUS HALL CONDUCTIVITY IN FERROMAGNETIC METALS

Before getting to our main result for the ATHC, we compare our result for the AHC with previous calculation results and experimental results to assess the reliability of our calculation. Figure 3 shows the intrinsic AHC (blue lines) and the side-jump AHC (red lines) of bcc Fe magnetized along [001] [Fig. 3(a)], fcc Ni magnetized along [111] [Fig. 3(b)], and Co magnetized along c axis [Fig. 3(c)] and along a axis [Fig. 3(d)]. The discrepancy of band structures between c-axis Co and a-axis Co leads to the anisotropy in the AHCs with respect to the magnetization direction.

Table I summarizes our results for the intrinsic and the side-jump AHCs at the true Fermi energy. We compare our results for AHC with previous theories in Appendix A and demonstrate that our calculation results for both intrinsic and side-jump AHCs at $T = 300$ K are quite close to the previous calculation results. Table I also includes experimentally

TABLE I. The theoretically calculated AHC (σ_{H} [$(\Omega\,\mathrm{cm})^{-1}$]) for Fe, Co, and Ni from the DFT+U calculation at $T = 300$ K. The temperature dependence of $\sigma_{\mathrm{H}}^{\mathrm{int}}$ and $\sigma_{\mathrm{H}}^{\mathrm{sj}}$ are negligible in our calculation scheme. Their sum $\sigma_{\mathrm{H}} = \sigma_{\mathrm{H}}^{\mathrm{int}} + \sigma_{\mathrm{H}}^{\mathrm{sj}}$ is compared with the experimentally measured AHC $\sigma_{\mathrm{H}}^{\mathrm{exp}}$.

	$\sigma_{\mathrm{H}}^{\mathrm{int}}$	$\sigma_{\mathrm{H}}^{\mathrm{sj}}$	σ_{H}	$\sigma_{\mathrm{H}}^{\mathrm{exp}}$
bcc Fe [001]	735	112	847	1032 ($T = 300$ K) [42]
fcc Ni [111]	−1332	−286	−1618	−646 ($T = 300$ K) [43]
				−1686 ($T = 5$ K) [44]
hcp Co (c axis)	629	201	829	813 [45]
hcp Co (a axis)	185	−62	123	150 [45]
hcp Co (poly)	333	26	359	340 [46]

measured AHCs in its last column for a detailed comparison, as discussed below.

The intrinsic contribution σ_H^{int} to the AHC is larger than the side-jump contribution σ_H^{sj} to the AHC. We thus compare σ_H^{int} with the experimentally obtained AHC σ_H^{exp}. For Fe, the calculated value $\sigma_{H,xy}^{int} = 735\ (\Omega\,\mathrm{cm})^{-1}$ reaches 70% of the experimental value $\sigma_{H,xy}^{exp} \approx 1032\ (\Omega\,\mathrm{cm})^{-1}$ [42] in [100] whiskers at $T = 300$ K. For Co, $\sigma_{H,xy}^{int} = 629\ (\Omega\,\mathrm{cm})^{-1}$ magnetized along c axis and $\sigma_{H,yz}^{int} = 185\ (\Omega\,\mathrm{cm})^{-1}$ magnetized along a axis reach 75% and 120% of the experimental values $\sigma_{H,xy}^{exp} \approx 813\ (\Omega\,\mathrm{cm})^{-1}$ and $\sigma_{H,yz}^{exp} \approx 150\ (\Omega\,\mathrm{cm})^{-1}$ [45], respectively. For Ni, $\sigma_H^{int} = -1332\ (\Omega\,\mathrm{cm})^{-1}$ is twice larger than the experimental value $\sigma_H^{exp} = -646\ (\Omega\,\mathrm{cm})^{-1}$ at $T = 300$ K [43].

When both the intrinsic and side-jump contributions to the AHC are taken into account, our results for Fe and Co align better with the experimental results at room temperature. The calculated value of the total AHC for bcc Fe [001] $\sigma_{H,xy} = \sigma_{H,xy}^{int} + \sigma_{H,xy}^{sj} = 847\ (\Omega\,\mathrm{cm})^{-1}$ reaches 85% of the experimental value $\sigma_{H,xy}^{exp} \approx 1032\ (\Omega\,\mathrm{cm})^{-1}$ [42] in [100] whiskers. We attribute this difference to the electron-electron interactions. Although the interaction effect is partially taken into account through U and J, this recipe does not fully capture the interaction effect. It was reported that considering the dynamically screened interaction into a Green function yields a band structure different from that obtained from the GGA [23]. For the modified band structure and eigenstates, the intrinsic AHC changes from $\sigma_{H,xy}^{int} = 735\ (\Omega\,\mathrm{cm})^{-1}$ to $\sigma_{H,xy}^{int} = 847\ (\Omega\,\mathrm{cm})^{-1}$. By combining this modified $\sigma_{H,xy}^{int}$ with the unmodified $\sigma_{H,xy}^{sj}$, we obtain the modified theoretical result of $\sigma_{H,xy} = 970\ (\Omega\,\mathrm{cm})^{-1}$, which reaches 95% of the experimental value [42].

For Co, the calculated AHC for c-axis Co $\sigma_{H,xy} = 829\ (\Omega\,\mathrm{cm})^{-1}$ and for a-axis Co $\sigma_{H,yz} = 123\ (\Omega\,\mathrm{cm})^{-1}$ are close to the experimental values $\sigma_{H,xy}^{exp} \approx 812\ (\Omega\,\mathrm{cm})^{-1}$ and $\sigma_{H,yz}^{exp} \approx 150\ (\Omega\,\mathrm{cm})^{-1}$ [45]. The agreement between theoretical and experimental values is reasonably good. The AHC of polycrystalline Co can be approximately evaluated by the weighted average of the AHC $\sigma_H(\theta = 0)$ magnetized along c axis ($\theta = 0$) and the AHC $\sigma_H(\theta = \pi/2)$ magnetized along a axis ($\theta = \pi/2$): $\sigma_{poly} \approx [\sigma_H(\theta = 0) + 2\sigma_H(\theta = \pi/2)]/3$. This approximation results in $\sigma_{poly} \approx 359\ (\Omega\,\mathrm{cm})^{-1}$, which is close to the experimental value of polycrystalline Co $\sigma_{H,poly}^{exp} \approx 340\ (\Omega\,\mathrm{cm})^{-1}$ [46].

For Ni, our calculation result $\sigma_H = -1618\ (\Omega\,\mathrm{cm})^{-1}$ is close to the experimental value $\sigma_H^{exp} = -1686\ (\Omega\,\mathrm{cm})^{-1}$ at at $T = 5$ K [44] but quite different from the measured value $\sigma_H^{exp} = -646\ (\Omega\,\mathrm{cm})^{-1}$ at $T = 300$ K [43]. The main cause for this difference is the electron-phonon interaction, which is not considered in our calculation. According to the previous calculation [24], Ni is particularly strongly affected by the electron-phonon interaction. Although the effect of the electron-phonon interaction on $\sigma_{H,xy}^{int}$ in Ni [111] has not been examined yet theoretically, the theoretical study on Ni [001] indicates the strong electron-phonon interaction effect on $\sigma_{H,xy}^{int}$ at $T = 0$ and $T = 300$ K; as the temperature increases from 0 to 300 K, the electron-phonon interaction becomes more significant and modifies the electron band structure so that $\sigma_{H,xy}^{int}$ is altered from $\sigma_H^{int} = -1100\ (\Omega\,\mathrm{cm})^{-1}$ at $T = 0$ to $\sigma_H^{int} = -500\ (\Omega\,\mathrm{cm})^{-1}$ at $T = 300$ K. In our calculation, however, the electron-phonon interaction has not been included. The electron-phonon interaction has a much weaker effect in Fe and Co than in Ni. For instance, Ref. [24] reported that $\sigma_{H,xy}^{int}$ of Fe increases from 707 $(\Omega\,\mathrm{cm})^{-1}$ at $T = 0$ to 770 $(\Omega\,\mathrm{cm})^{-1}$ at $T = 300$ K. Considering this increase in our $\sigma_{H,xy}^{int}$ with summation to $\sigma_{H,xy}^{sj}$, σ_H increases to 882 $(\Omega\,\mathrm{cm})^{-1}$ at $T = 300$ K, much closer to the experimental value $\sigma_H^{exp} = 1032\ (\Omega\,\mathrm{cm})^{-1}$ at the same temperature.

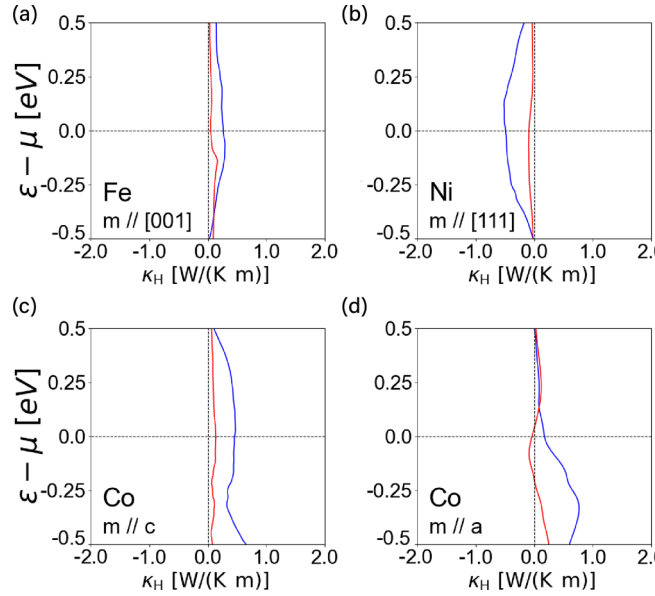

FIG. 4. The ATHC from the intrinsic mechanism (blue line) and the side-jump mechanism (red line) of bcc Fe [001] (a), fcc Ni [111] (b), and hcp Co magnetized along c axis (c) and a axis (d) at $T = 150$ K.

IV. ANOMALOUS THERMAL HALL CONDUCTIVITY IN FERROMAGNETIC METALS

We come to the main theme of the paper—the calculation of the anomalous portion of the thermal Hall conductivity in ferromagnetic metals. Figure 4 shows the intrinsic ATHC κ_H^{int} (blue lines) and the side-jump ATHC κ_H^{sj} (red lines) of bcc Fe magnetized along [001] [Fig. 4(a)], fcc Ni magnetized along [111] [Fig. 4(b)], and Co magnetized along c axis [Fig. 4(c)] and along a axis [Fig. 4(d)] according to the formulas in Eq. (2).

The ATHCs for these materials have not been obtained by other first-principle calculations, and we can only compare our results with the experimental values at two select temperatures, $T = 150$ K and $T = 300$ K. Table II summarizes the intrinsic and the side-jump ATHCs at the true Fermi level, along with the experimental values. Here, we obtain the polycrystalline ATHCs $\kappa_{H,poly}$ from $\kappa_H(\theta = 0)$ magnetized along c axis ($\theta = 0$) and the ATHC $\kappa_H(\theta = \pi/2)$ magnetized along a axis ($\theta = \pi/2$): $\kappa_{H,poly} \approx [\kappa_H(\theta = 0) + 2\kappa_H(\theta = \pi/2)]/3$. We first compare the intrinsic contribution for ATHC obtained by our calculations (κ_H^{int}) with that obtained from previous experiments ATHC (κ_H^{exp}). At $T = 150$ K, there are some discrepancies between κ_H^{int} and κ_H^{exp}; for Fe, the calculated

TABLE II. The ATHC {κ [W/(K m)]} for Fe, Co, and Ni from DFT+U calculation at $T = 150$ K and at $T = 300$ K.

T = 150 K	κ_H^{int}	κ_H^{sj}	κ_H	κ_H^{exp}
bcc Fe [001]	0.266	0.042	0.308	0.32 [13]
fcc Ni [111]	–0.493	–0.105	–0.598	–0.360 [14]
hcp Co (c axis)	0.230	0.070	0.300	
hcp Co (a axis)	0.067	–0.022	0.045	
hcp Co (polycrystals)	0.121	0.009	0.130	0.136 [14]
T = 300 K	κ_H^{int}	κ_H^{sj}	κ_H	κ_H^{exp}
bcc Fe [001]	0.523	0.083	0.606	0.63 [13]
fcc Ni [111]	–0.988	–0.196	–1.184	–0.357 [14]
hcp Co (c axis)	0.456	0.137	0.593	
hcp Co (a axis)	0.175	–0.034	0.141	
hcp Co (polycrystals)	0.269	0.023	0.292	0.249 [14]

value $\kappa_{H,xy}^{int} \approx 0.266$ W/(K m) reaches 83% of the experimental value $\kappa_{H,xy}^{exp} \approx 0.32$ W/(K m) [13]. For polycrystalline Co, the calculated value $\kappa_{H,xy}^{int} \approx 0.121$ W/(K m) reaches 90% of the experimental value $\kappa_{H,xy}^{exp} \approx 0.136$ W/(K m) [14]. In Ni, the calculated value $\kappa_{H,xy}^{int} \approx -0.493$ W/(K m) reaches 140% of the experimental value $\kappa_{H,xy}^{exp} \approx -0.360$ W/(K m) [14].

Next, we compare the calculated value of the total ATHCs $\kappa_H = \kappa_H^{int} + \kappa_H^{sj}$ with the experimental values κ_H^{exp}. For Fe and Co, the calculated value κ_H is excellent agreement with κ_H^{exp}. For Fe, the calculated value $\kappa_{H,xy} = 0.308$ W/(K m) and the experimental value $\kappa_{H,xy}^{exp} \approx 0.32$ W/(K m) are very close to each other. For polycrystalline Co, the calculated value $\kappa_H \approx 0.130$ W/(K m) and the experimental value $\kappa_H^{exp} \approx 0.136$ W/(K m) are again very close to each other. For Ni, however, the calculated value $\kappa_H \approx -0.598$ W/(K m) is significantly larger than the experimental value $\kappa_H^{exp} \approx -0.36$ W/(K m).

At $T = 300$ K, κ_H^{int}, κ_H^{sj}, and κ_H^{exp} for Fe and Co become almost doubled compared to the corresponding values at $T = 150$ K. This is expected since it is the ratio κ_H/T that serves as the intrinsic measure of thermal conduction rather than κ_H itself. For Fe, the calculated value $\kappa_{H,xy} \approx 0.606$ W/(K m) agrees with the experiment $\kappa_{H,xy}^{exp} \approx 0.63$ W/(K m). For Co, the agreement between κ_H and κ_H^{exp} still remains reasonably good. For polycrystalline Co, the calculated value $\kappa_{H,poly} \approx 0.292$ W/(K m) is slightly larger than the experimental value $\kappa_H^{exp} \approx 0.249$ (K m) [14]. But for Ni, the difference between the theoretical and the experimental value is considerably enlarged; the calculation value $\kappa_H \approx -1.184$ W/(K m) at $T = 300$ K is roughly twice larger than the corresponding value at $T = 150$ K, whereas the experimental value $\kappa_H^{exp} \approx -0.357$ (K m) at $T = 300$ K is almost equal to the corresponding value at $T = 150$ K [14]. We attribute the enlarged difference to the enlarged effect of the electron-phonon interaction at $T = 300$ K. For Fe and Co, the effect of electron-phonon interaction on κ_H seems negligible.

For all 3d ferromagnetic transition metals examined above, the intrinsic mechanism generates the most important contribution to the ATHC, similar to the situation for the AHC. Regarding the next most important contribution to the ATHC, the answer depends on the material as well as the temperature. For Fe and Co, the impurity-induced side-jump contribution is subdominant and helps to achieve excellent agreement between theoretical and experimental values, especially at the lower temperatures ($\leqslant$150 K). The situation is different for Ni. Adding the impurity-induced side-jump contribution to the intrinsic contribution widens the gap between theory and experiment, becoming worse at elevated temperatures ($\sim$300 K). Based on our experience with the AHC, we argue that an important source of this deviation is the electron-phonon interaction neglected in our calculation. This is supported by the observations that the deviation occurs only for Ni (the material that is the most significantly affected by the electron-phonon interaction, according to our investigation of the AHC in Sec. III) and that the deviation is enhanced with increasing temperature.

Another possible source of the discrepancy is the anomalous thermal Hall current carried by phonons or magnons, which we do not take into account. However, it is unlikely that these contributions are relevant in 3d ferromagnetic transition metal. For thermal Hall transport by phonons, applying an external magnetic field is a necessary ingredient [1,4,5] whereas here we are focused on magnetic metals at zero external magnetic field. For magnons, the magnon Berry curvature resulting from noncollinear spins in the ground state [6] is absent in 3d ferromagnetic transition metal since the magnetization there is collinear.

V. VALIDITY OF WIEDEMANN-FRANZ RELATION FOR AHC AND ATHC

The original Wiedemann-Franz law relates the longitudinal thermal conductivity κ with the longitudinal charge conductivity σ through the relation $L = \kappa/(\sigma \cdot T) = L_0 \equiv \pi^2/3(k_B/e)^2 = 2.44 \times 10^{-8}$ V^2 K^{-2}, where L_0 is the Sommerfeld value [47]. Later, this law was generalized to the anomalous transverse Wiedemann-Franz law [39] relating the ATHC κ_H with the AHC σ_H via $L_H = \kappa_H/(\sigma_H T)$. Strictly speaking, this law holds only when inelastic processes are vanishingly weak and thermal currents carried by excitations other than electrons are negligible [48]. In metallic systems, it is often assumed that this law remains approximately valid in a wide temperature range since electrons dominate both charge and energy transport and since the Fermi energy scale of electrons is much larger than characteristic energy scales of other quasiparticles such as phonons and magnons [14]. None of the existing considerations have made a careful examination of the consequence of realistic band structures of magnetic metals on the transverse Wiedemann-Franz law so far.

Here, we carefully examine its validity for 3d transition metals. The solid lines in Fig. 5 show the calculated L_H for bcc Fe [001] [Fig. 5(a)], fcc Ni [111] [Fig. 5(b)], hcp Co (c axis) [Fig. 5(c)]. For bcc Fe [001], L_H agrees excellently with L_0 in the entire temperature range examined (5 K to 300 K). Also, for fcc Ni [111], L_H stays close to L_0 in the entire temperature range up to 300 K. In contrast, for hcp Co L_H is close to L_0 only in the low-temperature range ($\leqslant$150 K) and shows an upward deviation from L_0 by as much as $0.1L_0$ at $T = 300$ K.

To examine the origin of the violation, we rewrite the intrinsic and impurity-scattering-originated side-jump contributions for AHC and ATHC in Eqs. (1a) and (1b) as

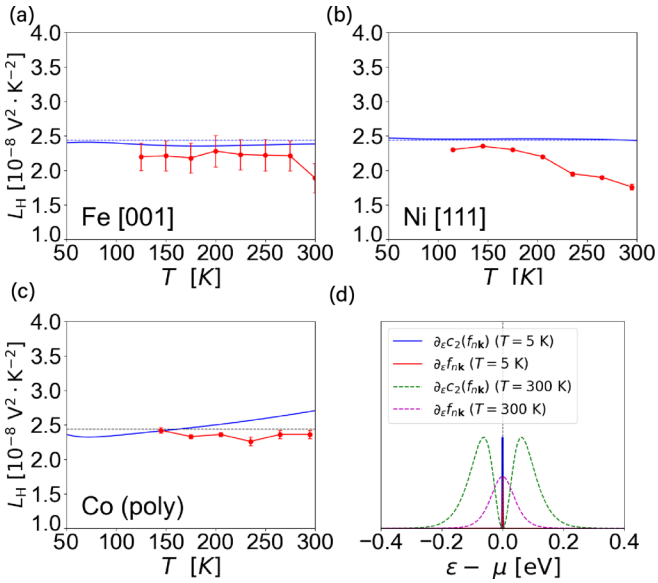

FIG. 5. The temperature dependence of the calculated results (blue line) and the experimental results (red dots) [14,48] of the transverse Lorenz ratio L_H for bcc Fe [001] (a), fcc Ni [111] (b), and polycrystalline hcp Co (c). The dotted lines are L_0. (d) The Fermi energy dependence of $\partial_\varepsilon f_{n\mathbf{k}}$ (red-solid line), $\partial_\varepsilon c_2(f_{n\mathbf{k}})$ (blue-solid line) at T = 5 K and $\partial_\varepsilon f_{n\mathbf{k}}$ (magenta-dotted line), $\partial_\varepsilon c_2(f_{n\mathbf{k}})$ (green-dotted line) at T = 300 K. The two curves overlap almost completely at 5 K.

follows:

$$\sigma^{\rm int}_{{\rm H},\alpha\beta} = \int d\varepsilon \partial_\varepsilon f(\varepsilon) \sigma^{{\rm int},0}_{{\rm H},\alpha\beta}(\varepsilon), \tag{4a}$$

$$\kappa^{\rm int}_{{\rm H},\alpha\beta} = \int d\varepsilon \partial_\varepsilon c_2(f(\varepsilon)) \sigma^{{\rm int},0}_{{\rm H},\alpha\beta}(\varepsilon), \tag{4b}$$

$$\sigma^{\rm sj}_{{\rm H},\alpha\beta} = \int d\varepsilon \partial_\varepsilon f(\varepsilon) \sigma^{{\rm sj},0}_{{\rm H},\alpha\beta}(\varepsilon), \tag{4c}$$

$$\kappa^{\rm sj}_{{\rm H},\alpha\beta} = \int d\varepsilon \partial_\varepsilon c_2(f(\varepsilon)) \sigma^{{\rm sj},0}_{{\rm H},\alpha\beta}(\varepsilon), \tag{4d}$$

where $\sigma^{{\rm int},0}_{{\rm H},\alpha\beta}(\varepsilon)$ and $\sigma^{{\rm sj},0}_{{\rm H},\alpha\beta}(\varepsilon)$ are, respectively, the intrinsic and impurity-scattering side-jump contributions for AHC at $T = 0$. The only difference in the AHC and ATHC formulas is the use of either $\partial_\varepsilon f(\varepsilon)$ or $\partial_\varepsilon c_2(f_{n\mathbf{k}})$ as distribution functions.

In the low-temperature range, both functions have a narrow single peak at $\varepsilon = \mu$ [solid curves in Fig. 5(d)]. One can show, in the lowest order of the Sommerfeld expansion for $\partial_\varepsilon f$ and $\partial_\varepsilon c_2$, that the Wiedemann-Franz relation holds as $\kappa_{{\rm H},\alpha\beta}(\mu)/(\sigma_{{\rm H},\alpha\beta}(\mu)\cdot T) = L_0$.

At elevated temperatures, $\partial_\varepsilon c_2(f_{n\mathbf{k}})$ develops into double peaks at $\varepsilon = \mu \pm \Delta$ ($\Delta \approx 2.5 k_{\rm B} T$). Again, to the leading order in the Sommerfeld expansion, we obtain

$$\frac{\kappa_{{\rm H},\alpha\beta}(\mu)}{T} \approx \frac{L_0}{2}\left[\sigma^0_{{\rm H},\alpha\beta}(\mu+\Delta) + \sigma^0_{{\rm H},\alpha\beta}(\mu-\Delta)\right]. \tag{5}$$

If AHC is further assumed to vary slowly so that $\sigma^0_{{\rm H},\alpha\beta}(\mu \pm \Delta) \approx \sigma^0_{{\rm H},\alpha\beta}(\mu)$, Wiedemann-Franz law holds. On the other hand, the leading-order Sommerfeld expansion breaks down at elevated temperatures and results in deviations from the strict Wiedemann-Franz relation.

Therefore, in materials where $\sigma^{{\rm int},0}_{{\rm H},\alpha\beta}(\varepsilon)$ or $\sigma^{{\rm sj},0}_{{\rm H},\alpha\beta}(\varepsilon)$ vary considerably with ε near $\varepsilon = \mu$, the value of $L_{\rm H}$ at elevated temperatures can deviate from L_0 considerably. This explains the deviation of the calculated $L_{\rm H}$ from L_0 for hcp Co. Indeed in Co (a axis), $\sigma^{{\rm int},0}_{{\rm H},\alpha\beta}(\varepsilon)$ and $\sigma^{{\rm sj},0}_{{\rm H},\alpha\beta}(\varepsilon)$ vary considerably with ε. The AHC $\sigma^{{\rm int},0}_{{\rm H},\alpha\beta}(\varepsilon)$ and $\sigma^{{\rm sj},0}_{{\rm H},\alpha\beta}(\varepsilon)$ in polycrystalline Co has qualitatively similar dependence on ε since the AHC in polycrystalline Co is the weighted average of the AHC in Co (c axis) and Co (a axis). In summary, we find the theory supports the validity of anomalous transverse Wiedemann-Franz law within 3.7%, 1.2%, and 10.8% accuracy for Fe, Ni, and Co, respectively, over all temperatures (< 300 K).

Next, we discuss the effect of the electron-phonon scattering on $L_{\rm H}$. When an electron collides with a phonon, the electron loses its energy both by drastically or barely losing its momentum [49]. The former decreases both charge and heat current, while the latter only decreases the heat current. This different scattering process can result in the violation of the anomalous transverse Wiedemann-Franz law at elevated temperatures.

We attempt to assess the electron-phonon scattering effect on $L_{\rm H}$ through experimental results. The solid circles in Figs. 5(a)–5(c) show that $L_{\rm H}$ stays close to the ideal value L_0 from the lowest available temperature to $T = 150$ K. At higher temperatures, $L_{\rm H}$ exhibits deviations from L_0. For bcc Fe [Fig. 5(a)] and fcc Ni [Fig. 5(b)], $L_{\rm H}$ decreases with increasing T. Such decreases are understandable considering that the electron-phonon scattering reduces the energy carried by electrons at elevated temperatures [13,14]. For hcp Co [Fig. 5(c)], however, $L_{\rm H}$ stays close to L_0 even at 300 K. We attribute this peculiar behavior to the competition of the two opposite trends: the tendency for electron-phonon scattering to reduce $L_{\rm H}$ below L_0 on one hand, and the tendency for $\sigma^{{\rm int},0}_{{\rm H},\alpha\beta}(\varepsilon)$ or $\sigma^{{\rm sj},0}_{{\rm H},\alpha\beta}(\varepsilon)$ to increase $L_{\rm H}$ above L_0 through the ε dependence on the other.

VI. CONCLUSIONS

We calculated the intrinsic and the impurity-scattering-induced side-jump contributions to the AHC and ATHC in elemental bcc Fe, hcp Co, and fcc Ni using the first-principle calculations through the DFT+U method. While the AHC of those materials has been investigated extensively before, there is very little study on ATHC, and what little is known about it has been inferred through Wiedemann-Franz law, whose validity remained uncertain. We found that the ATHC has the same qualitative dependence on the Fermi energy as the AHC. For Fe and Co, the sum of the intrinsic and the impurity-scattering-induced side-jump ATHCs match the known experimental values quite well, with the intrinsic contribution being dominant. The impurity-scattering-induced side-jump contribution is still considerable, but considering electron-phonon interaction can still enhance the accuracy of the total ATHC. In Ni, however, the effect of electron-phonon interaction is significant at elevated temperatures.

ACKNOWLEDGMENTS

We thank B. Choi for fruitful discussion. I.B. and H.-W.L. were supported by the Samsung Science and Tech-

nology Foundation (Grant No. BA-1501-51). J.H.H. was supported by the National Research Foundation of Korea (NRF) Grant funded by the Korean government (MSIT) (No. 2023R1A2C1002644). K.-W.K. was supported by the KIST Institutional Program. Supercomputing resources, including technical support, were provided by the Supercomputing Center, Korea Institute of Science and Technology Information (Contract No. KSC-2022-CRE-0468).

APPENDIX A: COMPARISON OF AHC TO PREVIOUS CALCULATIONS

The intrinsic AHC $\sigma^{\rm int}_{{\rm H},xy} = 735\ (\Omega\,{\rm cm})^{-1}$ at the true Fermi energy for bcc Fe [001] is in excellent agreement with $\sigma^{\rm int}_{{\rm H},xy} = 734\ (\Omega\,{\rm cm})^{-1}$ at $T = 300$ K obtained by the full-potential linearized augmented plane-wave method [17], $\sigma^{\rm int}_{{\rm H},xy} = 703\ (\Omega\,{\rm cm})^{-1}$ at $T = 300$ K by the norm-conserving pseudopotentials [50], and $\sigma^{\rm int}_{{\rm H},xy} = 750\ (\Omega\,{\rm cm})^{-1}$ obtained by the Korringa–Kohn–Rostoker Green's function method [24]. Our intrinsic AHC $\sigma^{\rm int}_{{\rm H},xy} \approx 629\ (\Omega\,{\rm cm})^{-1}$ for c-axis magnetized hcp Co and $\sigma^{\rm int}_{{\rm H},yz} = 185\ (\Omega\,{\rm cm})^{-1}$ for a-axis magnetized hcp Co are close to those in the previous AHC calculation $\sigma^{\rm int}_{{\rm H},xy} = 618\ (\Omega\,{\rm cm})^{-1}$ at $T = 0$ implemented by evaluating the static limit of magneto-optical conductivity [18] and $\sigma^{\rm int}_{{\rm H},yz} \approx 100\ (\Omega\,{\rm cm})^{-1}$ at $T = 0$ obtained by the full-potential linearized augmented plane-wave method [37]. Our intrinsic AHC $\sigma^{\rm int}_{\rm H} = -1332\ (\Omega\,{\rm cm})^{-1}$ for fcc Ni [111] agrees with the previous work $\sigma^{\rm int}_{\rm H} = -1200\ (\Omega\,{\rm cm})^{-1}$ at $T = 0$ obtained by the FLEUR code [37]. Although some of the previous calculation results are obtained at $T = 0$, it is still reasonable to compare these results with our calculation results at $T = 300$ K since the temperature dependence of $\sigma^{\rm int}_{\rm H}$ is weak in our calculation. It has been well known that $\sigma^{\rm int}_{\rm H}$ of Ni is sensitive to the correlation effects parameterized by U and J [31,37]. $\sigma^{\rm int}_{\rm H}$ changes from $-2000\ (\Omega\,{\rm cm})^{-1}$ at $U = 0$ to $-850\ (\Omega\,{\rm cm})^{-1}$ at $U = 3.9$ eV. $\sigma^{\rm int}_{\rm H}$ of Fe and Co are not sensitive to the correlation effects [18,24].

The side-jump AHCs in our study are also in good agreement with the previous calculation results [31,37] obtained by the full-potential linearized augmented plane-wave method. For bcc Fe [001], our side-jump contribution $\sigma^{\rm sj}_{{\rm H},xy} = 112\ (\Omega\,{\rm cm})^{-1}$ to the AHC is in excellent agreement to the previous result $\sigma^{\rm sj}_{{\rm H},xy} = 112\ (\Omega\,{\rm cm})^{-1}$ at $T = 300$ K. Our side-jump contribution to the AHC $\sigma^{\rm sj}_{{\rm H},xy} = 201(\Omega\,{\rm cm})^{-1}$ for c-axis hcp Co and $\sigma^{\rm sj}_{{\rm H},xy} = -62(\Omega\,{\rm cm})^{-1}$ for a-axis hcp Co are close to the previous calculation results $\sigma^{\rm sj}_{{\rm H},xy} = 201$, $\sigma^{\rm sj}_{{\rm H},yz} = -88\ (\Omega\,{\rm cm})^{-1}$ at $T = 300$ K. For fcc Ni [111], our side-jump contribution to the AHC $\sigma^{\rm sj}_{\rm H} = -286\ (\Omega\,{\rm cm})^{-1}$ agrees with the previous work $\sigma^{\rm sj}_{\rm H} = -250\ (\Omega\,{\rm cm})^{-1}$.

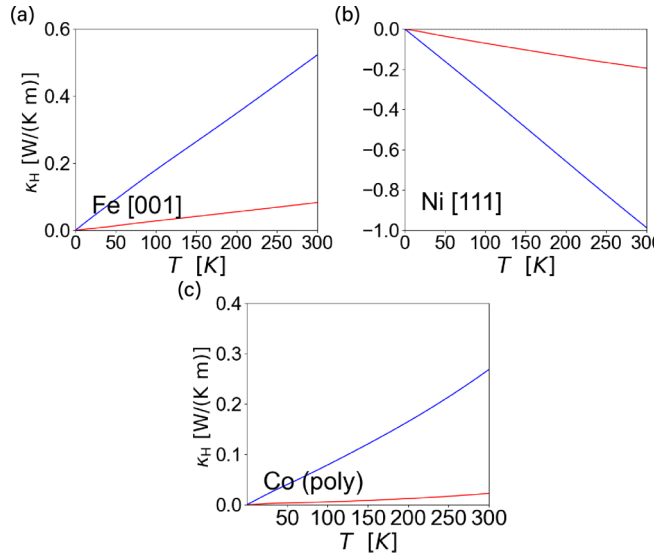

FIG. 6. The temperature dependence of the intrinsic (blue line) and the impurity-scattering side jump (red dots) contributions of the ATHC to the temperature for bcc Fe [001] (a), fcc Ni [111] (b), and polycrystalline hcp Co (c).

APPENDIX B: TEMPERATURE DEPENDENCE OF ATHC

Figure 6 shows the temperature dependence of the ATHC $\kappa_{\rm H}$ to the temperature T. The intrinsic $\kappa^{\rm int}_{\rm H}$ (blue line) and impurity-scattering side jump contributions $\kappa^{\rm sj}_{\rm H}$ (red line) are linearly proportional to T except for Co [Fig. 6(c)]. In Co, the linear dependence of the intrinsic contribution $\kappa^{\rm int}_{\rm H}$ to T is violated in $T > 150$ K as the same reason for the violation of the Wiedemann-Franz law.

[1] C. Strohm, G. L. J. A. Rikken, and P. Wyder, Phenomenological evidence for the phonon Hall effect, Phys. Rev. Lett. **95**, 155901 (2005).
[2] Y. Onose, T. Ideue, H. Katsura, Y. Shiomi, N. Nagaosa, and Y. Tokura, Observation of the magnon Hall effect, Science **329**, 297 (2010).
[3] Y. Kasahara, T. Ohnishi, Y. Mizukami, O. Tanaka, S. Ma, K. Sugii, N. Kurita, H. Tanaka, J. Nasu, Y. Motome *et al.*, Majorana quantization and half-integer thermal quantum Hall effect in a Kitaev spin liquid, Nature (London) **559**, 227 (2018).
[4] X. Li, B. Fauqué, Z. Zhu, and K. Behnia, Phonon thermal Hall effect in strontium titanate, Phys. Rev. Lett. **124**, 105901 (2020).
[5] G. Grissonnanche, S. Thériault, A. Gourgout, E. Boulanger, E. Lefrançois, A. Ataei, F. Laliberté, M. Dion, J.-S. Zhou, S. Pyon *et al.*, Chiral phonons in the pseudogap phase of cuprates, Nat. Phys. **16**, 1108 (2020).
[6] H. Katsura, N. Nagaosa, and P. A. Lee, Theory of the thermal Hall effect in quantum magnets, Phys. Rev. Lett. **104**, 066403 (2010).
[7] H. Lee, J. H. Han, and P. A. Lee, Thermal Hall effect of spins in a paramagnet, Phys. Rev. B **91**, 125413 (2015).
[8] J.-Y. Chen, S. A. Kivelson, and X.-Q. Sun, Enhanced thermal Hall effect in nearly ferroelectric insulators, Phys. Rev. Lett. **124**, 167601 (2020).

[9] H. Guo, D. G. Joshi, and S. Sachdev, Resonant thermal Hall effect of phonons coupled to dynamical defects, Proc. Natl. Acad. Sci. USA **119**, e2215141119 (2022).

[10] B. Flebus and A. H. MacDonald, Charged defects and phonon Hall effects in ionic crystals, Phys. Rev. B **105**, L220301 (2022).

[11] H. Doki, M. Akazawa, H.-Y. Lee, J. H. Han, K. Sugii, M. Shimozawa, N. Kawashima, M. Oda, H. Yoshida, and M. Yamashita, Spin thermal Hall conductivity of a kagome antiferromagnet, Phys. Rev. Lett. **121**, 097203 (2018).

[12] S. Onoda, N. Sugimoto, and N. Nagaosa, Quantum transport theory of anomalous electric, thermoelectric, and thermal Hall effects in ferromagnets, Phys. Rev. B **77**, 165103 (2008).

[13] Y. Shiomi, Y. Onose, and Y. Tokura, Extrinsic anomalous Hall effect in charge and heat transport in pure iron, $Fe_{0.997}Si_{0.003}$, and $Fe_{0.97}Co_{0.03}$, Phys. Rev. B **79**, 100404(R) (2009).

[14] Y. Shiomi, Y. Onose, and Y. Tokura, Effect of scattering on intrinsic anomalous Hall effect investigated by Lorenz ratio, Phys. Rev. B **81**, 054414 (2010).

[15] N. Nagaosa, J. Sinova, S. Onoda, A. H. MacDonald, and N. P. Ong, Anomalous Hall effect, Rev. Mod. Phys. **82**, 1539 (2010).

[16] L. Xu, X. Li, X. Lu, C. Collignon, H. Fu, J. Koo, B. Fauqué, B. Yan, Z. Zhu, and K. Behnia, Finite-temperature violation of the anomalous transverse Wiedemann-Franz law, Sci. Adv. **6**, eaaz3522 (2020).

[17] Y. Yao, L. Kleinman, A. H. MacDonald, J. Sinova, T. Jungwirth, D.-s. Wang, E. Wang, and Q. Niu, First principles calculation of anomalous Hall conductivity in ferromagnetic bcc Fe, Phys. Rev. Lett. **92**, 037204 (2004).

[18] J.-C. Tung, H.-R. Fuh, and G.-Y. Guo, Anomalous and spin Hall effects in hcp cobalt from GGA+U calculations, Phys. Rev. B **86**, 024435 (2012).

[19] H.-R. Fuh and G.-Y. Guo, Intrinsic anomalous Hall effect in nickel: A GGA +U study, Phys. Rev. B **84**, 144427 (2011).

[20] V. I. Anisimov, J. Zaanen, and O. K. Andersen, Band theory and Mott insulators: Hubbard U instead of Stoner I, Phys. Rev. B **44**, 943 (1991).

[21] B. Himmetoglu, R. M. Wentzcovitch, and M. Cococcioni, First-principles study of electronic and structural properties of CuO, Phys. Rev. B **84**, 115108 (2011).

[22] S. L. Dudarev, G. A. Botton, S. Y. Savrasov, C. J. Humphreys, and A. P. Sutton, Electron-energy-loss spectra and the structural stability of nickel oxide: An LSDA+U study, Phys. Rev. B **57**, 1505 (1998).

[23] E. Młyńczak, I. Aguilera, P. Gospodarič, T. Heider, M. Jugovac, G. Zamborlini, J.-P. Hanke, C. Friedrich, Y. Mokrousov, C. Tusche, S. Suga, V. Feyer, S. Blügel, L. Plucinski, and C. M. Schneider, Fe(001) angle-resolved photoemission and intrinsic anomalous Hall conductivity in Fe seen by different *ab initio* approaches: LDA and GGA versus *GW*, Phys. Rev. B **105**, 115135 (2022).

[24] D. Ködderitzsch, K. Chadova, J. Minár, and H. Ebert, Impact of finite temperatures and correlations on the anomalous Hall conductivity from *ab initio* theory, New J. Phys. **15**, 053009 (2013).

[25] C. Xiao, Y. Liu, M. Xie, S. A. Yang, and Q. Niu, Theory of the phonon side-jump contribution in anomalous Hall effect, Phys. Rev. B **99**, 245418 (2019).

[26] P. Giannozzi, S. Baroni, N. Bonini, M. Calandra, R. Car, C. Cavazzoni, D. Ceresoli, G. L. Chiarotti, M. Cococcioni, I. Dabo *et al.*, QUANTUM ESPRESSO: a modular and open-source software project for quantum simulations of materials, J. Phys.: Condens. Matter **21**, 395502 (2009).

[27] J. P. Perdew, K. Burke, and M. Ernzerhof, Generalized gradient approximation made simple, Phys. Rev. Lett. **77**, 3865 (1996).

[28] D. R. Hamann, Optimized norm-conserving Vanderbilt pseudopotentials, Phys. Rev. B **88**, 085117 (2013).

[29] H. J. Monkhorst and J. D. Pack, Special points for Brillouin-zone integrations, Phys. Rev. B **13**, 5188 (1976).

[30] I. Yang, S. Y. Savrasov, and G. Kotliar, Importance of correlation effects on magnetic anisotropy in Fe and Ni, Phys. Rev. Lett. **87**, 216405 (2001).

[31] J. Weischenberg, F. Freimuth, S. Blügel, and Y. Mokrousov, Scattering-independent anomalous Nernst effect in ferromagnets, Phys. Rev. B **87**, 060406(R) (2013).

[32] H. Mao, W. A. Bassett, and T. Takahashi, Effect of pressure on crystal structure and lattice parameters of iron up to 300 kbar, J. Appl. Phys. **38**, 272 (1967).

[33] F. Ono and H. Maeta, Determination of lattice parameters in hcp cobalt by using X-ray Bond's method, J. Phys. Colloq. **49**, 63 (1988).

[34] J. Bandyopadhyay and K. Gupta, Low temperature lattice parameter of nickel and some nickel-cobalt alloys and Grüneisen parameter of nickel, Cryogenics **17**, 345 (1977).

[35] G. Pizzi, V. Vitale, R. Arita, S. Blügel, F. Freimuth, G. Géranton, M. Gibertini, D. Gresch, C. Johnson, T. Koretsune *et al.*, Wannier90 as a community code: new features and applications, J. Phys.: Condens. Matter **32**, 165902 (2020).

[36] T. Qin, Q. Niu, and J. Shi, Energy magnetization and the thermal Hall effect, Phys. Rev. Lett. **107**, 236601 (2011).

[37] J. Weischenberg, F. Freimuth, J. Sinova, S. Blügel, and Y. Mokrousov, *Ab initio* theory of the scattering-independent anomalous Hall effect, Phys. Rev. Lett. **107**, 106601 (2011).

[38] A. A. Kovalev, J. Sinova, and Y. Tserkovnyak, Anomalous Hall effect in disordered multiband metals, Phys. Rev. Lett. **105**, 036601 (2010).

[39] L. Smrcka and P. Streda, Transport coefficients in strong magnetic fields, J. Phys. C: Solid State Phys. **10**, 2153 (1977).

[40] M. Jonson and G. D. Mahan, Mott's formula for the thermopower and the Wiedemann-Franz law, Phys. Rev. B **21**, 4223 (1980).

[41] M. J. Kearney and P. N. Butcher, Thermal transport in disordered systems, J. Phys. C: Solid State Phys. **21**, L265 (1988).

[42] P. N. Dheer, Galvanomagnetic effects in iron whiskers, Phys. Rev. **156**, 637 (1967).

[43] J. M. Lavine, Extraordinary Hall-effect measurements on Ni, some Ni alloys, and ferrites, Phys. Rev. **123**, 1273 (1961).

[44] L. Ye, Y. Tian, X. Jin, and D. Xiao, Temperature dependence of the intrinsic anomalous Hall effect in nickel, Phys. Rev. B **85**, 220403(R) (2012).

[45] E. Roman, Y. Mokrousov, and I. Souza, Orientation dependence of the intrinsic anomalous Hall effect in hcp cobalt, Phys. Rev. Lett. **103**, 097203 (2009).

[46] Y. Omori, E. Sagasta, Y. Niimi, M. Gradhand, L. E. Hueso, F. Casanova, and Y. C. Otani, Relation between spin Hall effect and anomalous Hall effect in 3*d* ferromagnetic metals, Phys. Rev. B **99**, 014403 (2019).

[47] N. W. Ashcroft and N. D. Mermin, *Solid State Physics* (Holt-Saunders, Philadelphia, 1976).

[48] X. Li, L. Xu, L. Ding, J. Wang, M. Shen, X. Lu, Z. Zhu, and K. Behnia, Anomalous Nernst and Righi-Leduc effects in Mn_3Sn: Berry curvature and entropy flow, Phys. Rev. Lett. **119**, 056601 (2017).

[49] J. M. Ziman, *Principles of the Theory of Solids*, 2nd ed. (Cambridge University Press, Cambridge, 1972).

[50] X. Wang, D. Vanderbilt, J. R. Yates, and I. Souza, Fermi-surface calculation of the anomalous Hall conductivity, Phys. Rev. B **76**, 195109 (2007).